

Supplementary Information for

Industrial-era Decline in Arctic Methanesulfonic Acid is Offset by Increased Biogenic Sulfate Aerosol

Ursula A. Jongebloed^{1*}, Andrew J. Schauer², Jihong Cole-Dai³, Carleigh G. Larrick³, William C. Porter⁴, Lina Tashmim⁴, Sara Salimi¹, Shana R. Edouard¹, Lei Geng⁵, and Becky Alexander^{1*}

¹ Department of Atmospheric Sciences, University of Washington, Seattle, WA, USA

² Department of Earth and Space Sciences, University of Washington, Seattle, WA, USA

³ Department of Chemistry and Biochemistry, South Dakota State University, Brookings, SD, USA

⁴ Department of Environmental Science, University of California Riverside, Riverside, CA, 92507

⁵ School of Earth and Space Sciences, University of Science and Technology of China, Hefei, Anhui, China

*Ursula Jongebloed, Becky Alexander

Email: ujongebl@uw.edu, beckya@uw.edu

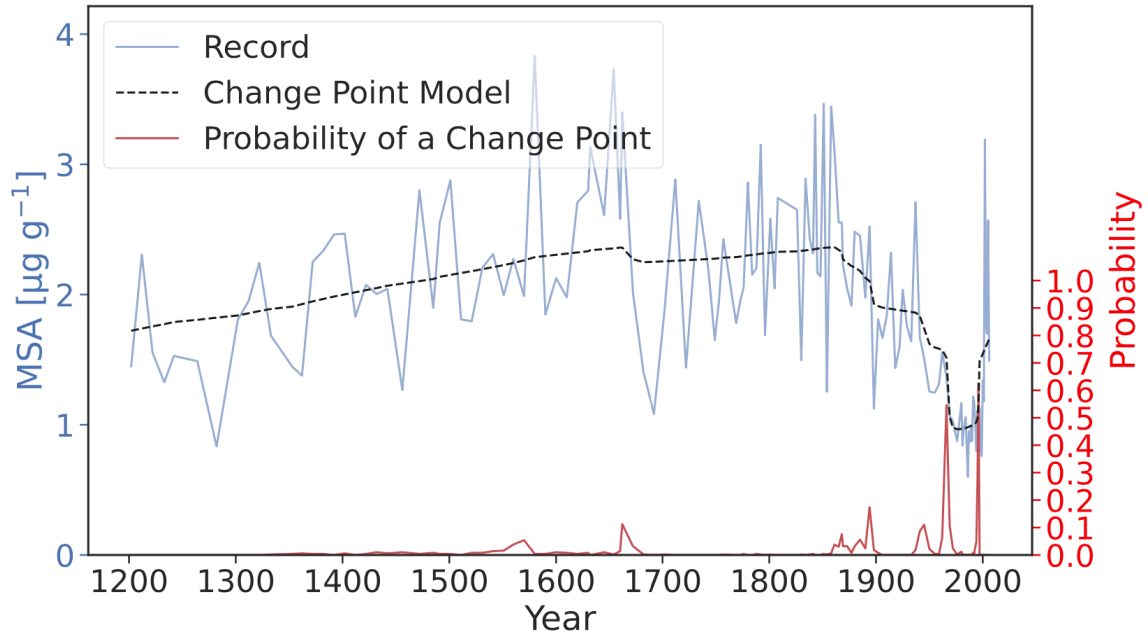


Figure S1. Bayesian Change Point Analysis of ice core MSA concentrations (blue line) from Summit, Greenland from 1200 to 2006 CE following Ruggieri (1). The blue line shows annual MSA concentration measurements once per decade from 1200 to 1750, once every four years from 1750 to 1980, and annually from 1980 to 2006. The recursive Bayesian change point algorithm from Ruggieri (1) identifies change points (red lines), which are changes in the parameters of a regression model used to describe a climatic time series. We assume a maximum of 6 change points in the ice core annual records since 1200 CE, a minimum separation time of 10 years between adjacent change points, and a linear fit in each identified regime. We sample 500 samples independently from the posterior distribution and calculate the best fit change point model (black line) (1). Due to the decadal and sub-decadal resolution of this record, the pre-1980 change points should be considered only as precise as the sampling resolution. The change points with greater than 15% probability occur at 1894, 1969, and 1996.

Supplementary Text S1: Ice core measurements

Methods for sample selection and ice core measurements are described in detail in Jongebloed et al. (2) and summarized in this section. Four shallow ice cores were collected in Summit, Greenland in 2007. Each core was analyzed for concentrations of major ions with continuous flow analysis using ion chromatography (3) and dated using annual layer counting. For sulfur isotope analysis in this study and Jongebloed et al. (2, 4), samples were selected during years without major volcanic eruptions (5) once per ten years at 1- to 2-year resolution from 1200 to 1750, once per four years at 1-year resolution from 1750 to 1980, and every year at 1-year resolution from 1980 to the top of the core (2006). In addition to samples selected during non-eruptive (or “background”) year during the preindustrial, an additional 13 years containing large volcanic eruptions were combined into 6 samples to characterize the volcanic isotopic signature of volcanic sulfur (see Supplementary Text S3a).

Following sample selection, sulfate in each sample was concentrated from a 1- to 2-liter volume to a 3-mL volume using an anion-exchange method that has no effect on $\delta^{34}\text{S}(\text{SO}_4^{2-})$ and has been previously used in with other $\delta^{34}\text{S}(\text{SO}_4^{2-})$ analyses (6). The concentrated solution was mixed with BaCl_2 to precipitate the sulfate as BaSO_4 , collected on a quartz filter paper, and packed into a tin capsule to be analyzed in a stable isotope mass spectrometer (7). $\delta^{34}\text{S}$ values were normalized to the Vienna Canyon Diablo Troilite (VCDT) scale using four in-house reference materials that are regularly calibrated against the international reference materials IAEA-S-1, IAEA-S-3, and NBS-127.

To estimate the uncertainty in our $\delta^{34}\text{S}$ measurements, we measured “whole-process standards” by dissolving an in-house sodium sulfate standard into a 1- to 2-liter volume of 18 M Ω water and measuring $\delta^{34}\text{S}$ using the same process applied to ice core samples. We binned all whole-process standards by size (e.g. 1 μg vs. 10 μg) because there is a size-dependent $\delta^{34}\text{S}$ measurement curve in stable isotope mass spectrometer measurements and took the standard deviation of the size-corrected whole process standard for each size bin. This resulted in an error estimate of ± 1.20 ‰. However, we note that duplicate and triplicate measurements of ice core samples resulted in a much smaller uncertainty of ± 0.02 ‰. Measuring the standards without preprocessing yields an uncertainty of ± 0.4 ‰. We use the larger uncertainty estimate to obtain a more conservative error bound. Using the $\delta^{34}\text{S}$ measurements and uncertainty in isotopic source signatures (described in Supplementary Text S3), we estimate concentrations of sulfate from each source and the uncertainty in source sulfate concentration by propagating the error from measurement uncertainty and source signature uncertainty.

Supplementary Text S2: Sources of Arctic Sulfate

The main sources of Arctic and global sulfate are sea salt, volcanoes, phytoplankton DMS emissions, and anthropogenic sources (e.g., fossil fuel burning) (8–12). Fluctuations in these sources can cause fluctuations in $\delta^{34}\text{S}(\text{nssSO}_4^{2-})$; for example, higher volcanic eruption frequency and higher passive volcanic degassing causes lower $\delta^{34}\text{S}(\text{nssSO}_4^{2-})$ and higher volcanic sulfate concentrations in the early 1200s (5, 13). However, other minor sources of sulfate such as terrestrial dust could influence ice core sulfate. Here we estimate the influence of terrestrial dust on ice core sulfate concentration and sulfur isotopic composition following Uemura et al. (14).

The contribution of terrestrial dust sulfate to nssSO_4^{2-} in the ice core can be estimated (13) by calculating the fraction of non-sea-salt calcium (nssCa^{2+}) in each ice core sample:

$$\begin{aligned} f_{\text{ssCa}} &= 0.025 \cdot [\text{Na}^+] / [\text{Ca}^{2+}] \\ [\text{nssCa}^{2+}] &= [\text{Ca}^{2+}] \cdot (1 - f_{\text{ssCa}}), \end{aligned}$$

where f_{ssCa} is the fraction of calcium attributed to sea salt and 0.025 is the molar concentration ratio of sea-salt sodium to calcium in ice core samples (14). These calculations yield a mean Summit ice core f_{ssCa} of 1.5% between 1200 and 1850 CE. The concentration of sulfate attributable to dust is:

$$[\text{SO}_4^{2-}]_{\text{terr}} = m \cdot [\text{nssCa}^{2+}],$$

where m is the molar concentration ratio of sulfate to calcium in dust. The soil global mean m value of 0.06-0.08 (41) has been used in many polar studies (4, 42–44). Bory et al. (15) estimate the mineralogical composition of dust at Summit to be illite (66%), chlorite (21%), kaolinite (8%), and smectite (5%). The contribution from high-sulfur minerals, such as calcite and gypsum, are negligible. The chemical formulas of illite, chlorite, kaolinite, and smectite indicate no sulfate contribution from these minerals (16). Therefore, we suggest that a standard value for m , such as 0.06-0.08, is appropriate for the Arctic, indicating that less than 3% of nssSO_4^{2-} in Summit ice core samples is attributable to dust.

If we assume that less than 3% of nssSO_4^{2-} is attributable to dust, and assume that dust sulfur isotopic composition spans a conservatively wide range similar to Southern Hemispheric dust of +5.1 to +19.5 ‰ (14), we solve for the average f_{volc} and f_{bio} in the preindustrial and industrial ice core samples using a modified version of the equation in methods:

$$\begin{aligned} f_{\text{bio}} + f_{\text{volc}} + f_{\text{terr}} &= 1, \text{ and} \\ f_{\text{bio}} \cdot \delta^{34}\text{S}_{\text{bio}} + f_{\text{volc}} \cdot \delta^{34}\text{S}_{\text{volc}} + f_{\text{terr}} \cdot \delta^{34}\text{S}_{\text{terr}} &= \delta^{34}\text{S}(\text{nssSO}_4^{2-}), \end{aligned}$$

where f_{terr} is the fraction of terrestrial dust sulfate ($f_{\text{terr}} = 0.03$) and $\delta^{34}\text{S}_{\text{terr}}$ is the sulfur isotopic signature of terrestrial dust sulfate. In the industrial era samples, anthropogenic sulfur fraction and isotopic composition is included in both equations. After subtracting out dust sulfate from $\delta^{34}\text{S}(\text{nssSO}_4^{2-})$ using the full range for $\delta^{34}\text{S}_{\text{terr}}$ of +5.1 to +19.5 ‰, we find that f_{volc} and f_{bio} change by less than 4% in the preindustrial and f_{volc} , f_{bio} , and f_{anthro} change by less than 4% in the industrial. We therefore conclude that dust exerts a negligible influence on Summit, Greenland ice core sulfate and sulfur isotopic composition.

Iizuka et al. (17) found an increase in calcium concentrations in a Southeast Dome, Greenland ice core from 2000 to 2014. Although this trend may indicate increased regional dust emissions influencing Southeast Dome, no statistically significant trend in calcium concentrations is observed in the Summit, Greenland ice core from 2000 to 2006 ($p = 0.23$) and the 2000 to 2006 ice core calcium concentrations are not statistically significantly different from the average preindustrial (1200 to 1850) calcium concentration ($p = 0.21$) (Figure S5).

Supplementary Text S3: Sulfur isotopic source signature determination

To attribute ice core sulfate to different sources using sulfur isotopes, we must estimate the sulfur isotopic signature of each source. To determine the sulfur isotopic signature of each source, we apply two methods: a Keeling Plot over the ice cores samples and statistical analysis of a compilation of direct sulfur isotopic measurements from each source. The isotopic signatures and methods are presented in Jongebloed et al. (2, 4) and described briefly below. We compare estimates from the two methods to each other and to previous estimates of each source signature to evaluate the accuracy of each signature. The Keeling Plots for volcanic and anthropogenic sulfur are presented in Jongebloed et al. (2, 4) shown in Figure S4a and S4b, the compilation of direct sulfur isotopic measurements from each source are presented in Jongebloed et al. (2, 4) and shown in Figure S4c, S4d, and S4e.

A Keeling plot is a regression of $\delta^{34}\text{S}(\text{nssSO}_4^{2-})$ measurements against the reciprocal of the concentration measurements ($1/[\text{nssSO}_4^{2-}]$) (18–20). The basis for the Keeling Plot is conservation of mass, where a constant background concentration and isotopic composition of atmospheric sulfate are influenced by variable emissions from another source (called the “variable source”) (18–20). The source signature of the variable source is the geometric mean intercept of the regression (18–20). For the Keeling Plot to be a valid method for determining an isotopic source signature, fluctuations in the relative magnitude of the variable source must be the dominant source of variability in concentration and isotopic composition of atmospheric sulfate (as opposed to fluctuations in isotopic source signature, meteorological variables, and background concentration and isotopic composition) (18–20). In the real world, the variable source is not a single emitter a population of emitters (e.g., several volcanoes or many coal-burning powerplants). Consequently, we characterize the source with population statistics; i.e., the mean and standard deviation. In this case, the population is characterized by the intercept of the Keeling Plot regression and the standard error of the intercept (18–20).

We discuss the applicability of the Keeling Plot to determine the isotopic composition of volcanic sulfate in Supplementary Text S3a and anthropogenic sulfate in Supplementary Text S3c. The Keeling Plot is not applicable to biogenic sulfate because biogenic sulfur emissions are less variable than volcanic (varying by more than an order of magnitude over the preindustrial and industrial eras) and anthropogenic sulfate (varying by a factor of three in the industrial era).

For the second method of determining isotopic signatures, we show compiled direct measurements of source materials from prior studies. This compilation is shown in detail in Jongebloed et al. (2, 4). We compile direct measurements of volcanic gases to determine $\delta^{34}\text{S}_{\text{volc}}$, direct measurements of coal and oil to determine $\delta^{34}\text{S}_{\text{anth}}$, and direct measurements of DMS and DMS oxidation products or precursors to determine $\delta^{34}\text{S}_{\text{bio}}$. More detailed descriptions for compilation of measurements of each source can be found in Supplementary Text S3a, S3b, S3c, and previously published studies by Jongebloed et al. (2, 4). With these compilations of direct measurements, we determine the mean and standard error of the mean for each source signature compilation. We are interested in the mean because we consider a source that is comprised of many disparate sources to be a population of sulfur sources (e.g., many volcanoes comprise the volcanic sulfur source, many coal and oil burning processes comprise the anthropogenic source, and many phytoplankton comprise the biogenic source). To

determine how each sulfur source influences total sulfate concentration and isotopic composition in the ice core, we calculate the mean sulfur isotopic composition of each compilation of measurements. We estimate the standard error of the mean, which indicates how different the “true” population mean is likely to be from the sample mean, using a bootstrapping method by resampling with replacement one thousand times and taking the mean of each resample. We use a bootstrapping method because we cannot assume that each source is normally distributed. However, if we do assume each source is normally distributed, we obtain the same standard error of the mean for each source (± 0.3 ‰ for $\delta^{34}\text{S}_{\text{anthro}}$, ± 0.7 ‰ for $\delta^{34}\text{S}_{\text{volc}}$, and ± 0.3 ‰ for $\delta^{34}\text{S}_{\text{bio}}$). Tables summarizing the compiled datasets for volcanic and biogenic source signatures are in Jongebloed et al. (2) and for anthropogenic source signature is in Jongebloed et al. (4).

Supplementary Text S3a: Volcanic sulfur isotopic source signature

Volcanic $\delta^{34}\text{S}$ varies by volcanic source depending on the isotopic composition of the mantle source, oxidation state of the magmatic sulfur and volcanic plume, sulfur species collected in the sample, and temperature of degassing (21). The volcanic sulfur isotopic signature applied to sulfate source apportionment varies from 0 to +5 ‰ in previous studies (12, 14, 22–24) based on a compilation of measurements from volcanoes around the world in Nielsen et al. (24). To determine $\delta^{34}\text{S}_{\text{volc}}$ from the volcanoes influencing Summit, we use the geometric mean regression of a Keeling Plot over our preindustrial volcanic eruption samples and non-eruptive “background” samples (Figure S3b), where we assume that DMS-derived biogenic sulfate provides a relatively steady source of sulfate during the preindustrial and volcanic degassing provides a more variable source of sulfate. We apply a Monte Carlo routine over the Keeling Plot to equally weight the eruptive and non-eruptive samples in each Keeling Plot regression. We estimate the error by calculating the standard error of the linear regression intercept without a Monte Carlo routine (± 0.5 ‰), which is the standard practice for estimating error in Keeling Plot determination of isotopic signatures (18). Using a Monte Carlo routine over the Keeling Plot regression does not result in a statistically significantly different estimate for $\delta^{34}\text{S}_{\text{volc}}$ when compared to a regression without a Monte Carlo routine ($+4.1 \pm 0.5$ ‰ vs. $+4.2 \pm 0.5$ ‰; Figure S3b), but we perform calculations with the signature estimated using a Monte Carlo routine ($\delta^{34}\text{S}_{\text{volc}} = +4.1 \pm 0.5$ ‰) because this method equally weights eruptive samples with the non-eruptive background samples.

We compare $\delta^{34}\text{S}_{\text{volc}} = +4.1 \pm 0.5$ ‰ to direct measurements of volcanic gases in Jongebloed et al. (2) (shown again here in Figure S3c). A compilation of 367 measurements of volcanic $\delta^{34}\text{S}(\text{H}_2\text{S})$, $\delta^{34}\text{S}(\text{SO}_4^{2-})$, $\delta^{34}\text{S}(\text{SO}_2)$, and $\delta^{34}\text{S}(\text{bulk S})$ from 38 volcanoes around the world has a mean $\delta^{34}\text{S}_{\text{volc}}$ of $+3.8 \pm 0.7$ ‰, where the standard error of the mean is determined by a bootstrapping method. Assuming these measurements are normally distributed also results in a standard error of the mean of ± 0.7 ‰. A value for $\delta^{34}\text{S}_{\text{volc}}$ of $+3.8 \pm 0.7$ ‰, which is determined independently from the Keeling Plot signature, is statistically indistinguishable from the source signature determined by the Keeling Plot. However, the compilation of volcanic gas measurements includes volcanoes that do not influence sulfate deposited at Summit Greenland. Thus, we use the Keeling Plot determination of $\delta^{34}\text{S}_{\text{volc}} = +4.1 \pm 0.5$ ‰ in the ice core sulfate source apportionment calculations.

It is possible that $\delta^{34}\text{S}_{\text{volc}}$ of volcanic sulfur emissions influencing sulfate at Summit could be variable over time; however, the regression analysis ($r = -0.68$ and $p = 0.0008$) in the

Keeling plot suggests otherwise. As individual volcanoes and volcanic regions vary in their emissions levels (e.g., from passive to eruptive), the factors affecting $\delta^{34}\text{S}_{\text{volc}}$ could vary, such as magma and plume oxidation state, sulfur speciation, and temperature (21, 25). However, there are no long-term studies of $\delta^{34}\text{S}_{\text{volc}}$ measured from a volcano or volcanic region that can constrain how variable $\delta^{34}\text{S}_{\text{volc}}$ can be in a region over time. Future studies could improve sulfate source apportionment by analyzing this variability; but until then, we use a Keeling Plot, which includes ice core samples from non-eruptive years spanning 850 years and eruption years spanning 500 years (Figure S3b).

Supplementary Text S3b: Biogenic sulfur isotopic source signature

A Keeling Plot cannot be used to determine $\delta^{34}\text{S}_{\text{bio}}$ because marine biogenic DMS is a less variable source of sulfur compared to volcanic and anthropogenic sulfur emissions, and Keeling Plots can only be used to determine the source signature of highly variable emission sources. Accordingly, we compile direct $\delta^{34}\text{S}$ measurements of marine biogenic compounds that are precursors to or oxidation products of phytoplankton DMS, including dimethylsulfoniopropionate (DMSP), which is a precursor to DMS; MSA, which is a minor product of DMS oxidation; and marine aerosol non-sea salt sulfate (nssSO_4^{2-}), which is the major product of DMS oxidation (Figure S3a). The compilation of these measurements is presented in Jongebloed et al. (2). The mean value for $\delta^{34}\text{S}_{\text{bio}}$ is $+18.8 \pm 0.3 \text{ ‰}$, where the error is the standard error of the mean determined by a bootstrapping method. Assuming these measurements are normally distributed rather than using a bootstrapping method results in a standard error of the mean of $\pm 0.3 \text{ ‰}$.

The value for $\delta^{34}\text{S}_{\text{bio}}$ used in numerous other sulfur isotope studies (9–12, 26) is estimated based on observations of $\delta^{34}\text{S}$ in sulfate from an inland Antarctic ice core (South Pole) far from the marine biogenic source of DMS (22), which provides an estimate of $+18.6 \pm 0.9 \text{ ‰}$. This previous estimate is statistically indistinguishable from our estimate of $+18.8 \pm 0.3 \text{ ‰}$, but is based on only two ice core samples, so we proceed with using our estimate for $\delta^{34}\text{S}_{\text{bio}}$ because it is calculated from 309 measurements of DMSP, DMS, MSA, and nssSO_4^{2-} from marine locations around the world (Figure S3a).

It is unlikely that $\delta^{34}\text{S}_{\text{bio}}$ has changed over the period of this study (1200 to 2006 CE). The value from $\delta^{34}\text{S}_{\text{bio}}$ is expected to be closely linked to the value for $\delta^{34}\text{S}_{\text{sea salt}}$ because DMS and DMSP are derived from dissolved sulfate in marine environments (27). Although $\delta^{34}\text{S}_{\text{sea salt}}$ can change over geological time scales (24), measurements of sea salt $\delta^{34}\text{S}$ over the past fifty years have shown consistent values for $\delta^{34}\text{S}_{\text{sea salt}}$ of $+21 \text{ ‰}$ (28–30). It is possible that changes to phytoplankton could result in small changes to $\delta^{34}\text{S}_{\text{bio}}$, but measurements of marine DMS, DMS precursors, and DMS oxidation products show consistent values over geographic regions (27) and over studies ranging from 1991 to 2017, based on the compilation of 309 measurements presented in Jongebloed et al. (2).

Supplementary Text S3c: Anthropogenic sulfur isotopic source signature

To estimate $\delta^{34}\text{S}_{\text{anthro}}$, we use a Keeling Plot of industrial era ice core samples (1850 to 2006 CE) not including years with major volcanic eruptions (e.g., Pinatubo in 1991) (Figure S3d). We do not employ a Monte Carlo method to estimate the intercept

because we measured numerous ice core samples with anthropogenic influence ($n = 61$). The geometric mean intercept provides an estimate for $\delta^{34}\text{S}_{\text{anthro}}$ of $+2.9 \pm 0.3 \text{ ‰}$, where the uncertainty is estimated from the standard error of the linear regression without a Monte Carlo or bootstrapping routine, which is the standard practice for determining the uncertainty in Keeling Plot determination of source signatures (18). The strong linear relationship between $\delta^{34}\text{S}(\text{nssSO}_4^{2-})$ and $1/[\text{nssSO}_4^{2-}]$ ($r = -0.80$, $p = 6.3 \times 10^{-15}$) and alignment between this estimate and previous estimates for $\delta^{34}\text{S}_{\text{anthro}}$ of (11, 31, 32) supports this determination of the anthropogenic source signature.

To further examine the anthropogenic source signature, we also compile 1,969 measurements of coal and oil $\delta^{34}\text{S}$ into 1,012 samples (where measurements are combined into a sample if they originate from the same source, e.g., the same oil well or are duplicate measurements of the same piece of coal) and analyze the mean statistics in detail in Jongebloed et al. (4) (shown here again in Figure S3e). The mean and standard error of the mean are $+3.4 \pm 0.3 \text{ ‰}$. The result is $+3.4 \pm 0.3 \text{ ‰}$ whether determined via bootstrapping or via assuming a normal distribution. This result is statistically indistinguishable from the Keeling Plot determination of $\delta^{34}\text{S}_{\text{anthro}} = +2.9 \pm 0.3 \text{ ‰}$. Because this compilation encompasses anthropogenic emissions from regions that do not impact sulfate deposition at Summit, Greenland air mass source region, and is only as comprehensive as the body of literature providing $\delta^{34}\text{S}$ measurements of coal and oil, we perform calculations with the signature of $\delta^{34}\text{S}_{\text{anthro}} = +2.9 \pm 0.3 \text{ ‰}$ (Figure S3d), which is more likely to be representative of the anthropogenic sulfur reaching the ice core location.

Although it is possible that this signature changes over time, especially as regions burned different relative amounts of coal and oil, we find that the coal and oil signature are similar ($\delta^{34}\text{S}_{\text{coal}} = +2.4 \pm 0.4 \text{ ‰}$ vs. $\delta^{34}\text{S}_{\text{oil}} = +3.7 \pm 0.4 \text{ ‰}$). Furthermore, this variability is captured by the Keeling Plot determination of the mean $\delta^{34}\text{S}_{\text{anthro}}$, which shows a strong linear relationship over the industrial era ($r = -0.80$, $p = 6.3 \times 10^{-15}$). Finally, alignment between this estimate and previous estimates for $\delta^{34}\text{S}_{\text{anthro}}$, which span over forty years (11, 31, 32), support a tightly constrained value for $\delta^{34}\text{S}_{\text{anthro}}$.

Supplementary Text S3d: Uncertainty analysis and limitations to source signature determination

The standard method used to estimate the uncertainty in a source signature determined via a Keeling Plot is the standard error of the intercept of the regression (18). The standard error of the intercept is used in the uncertainty estimates (i.e., error bars) shown in main text Figure 3, and the 95% confidence interval of the regression is shown as a shaded region in Figures S4b and S4d. To provide a larger uncertainty range, we also estimate prediction intervals of the Keeling Plot regression in Figures S4b and S4d. A prediction interval is a regression model that is intended to represent the 95% confidence interval in which the value of a future observation might fall (33). In other words, we are 95 percent confident that a single new observation from the preindustrial (Figure S4b) and industrial era (Figure S4d) would fall between the dashed lines showing the prediction interval. The range of intercepts shown by the prediction interval likely overestimates the uncertainty in the source signature determined via Keeling Plot because the majority of the variability in each observation is caused by a variability in the fluxes of the biogenic, volcanic, and anthropogenic sources (Figure S4d) rather than

variation in the source signatures. The 95% confidence interval of the Keeling Plot regression indicates the likely range of the mean volcanic (Figure S4b) and anthropogenic (Figure S4d) source signatures by estimating the 95% confidence interval of y-intercept, which is inherently a flux-weighted mean signature of volcanic (Figure S4b) and anthropogenic (Figure S4d) sources influencing the ice core region.

We note that adding larger error bars based on the prediction intervals to Figure S6b and S6d does not affect statistics discussed in the results of the main text. In the main text, we compare the preindustrial to the industrial era, for example, by computing the mean and standard deviation of the concentrations and ratios in these time periods. The mean and standard deviation of concentrations and ratios are not affected by the magnitude of the error bars in Figures 3 vs. Figure S6. The standard deviation of the concentrations and ratios is a conservative estimate of the uncertainty. If we estimate the uncertainty the equation $\sigma^2 = \sum_{i=1}^n \left(\frac{1}{n}\right)^2 \sigma_i^2$, where σ_i is each error bar in Figure 3 or Figure S6, the uncertainty is smaller. For example, the mean + std dev of bioSO₄ concentration in the preindustrial is $3.2 \pm 1.0 \mu\text{g S kg}^{-1}$ and the mean + $\sqrt{\sum_{i=1}^n \left(\frac{1}{n}\right)^2 \sigma_i^2}$ of bioSO₄ concentration in the preindustrial is $3.2 \pm 0.1 \mu\text{g S kg}^{-1}$ (using error bars from Figure 3) or $3.2 \pm 0.3 \mu\text{g S kg}^{-1}$ (using prediction interval error bars from Figure S6).

We do not use the compilations of $\delta^{34}\text{S}_{\text{volc}}$ and $\delta^{34}\text{S}_{\text{anthro}}$ in Figures S4c and S4e to estimate the biogenic sulfate concentration in the main text Figure 3 because these compilations do not present a flux-weighted, regionally representative source signature for $\delta^{34}\text{S}_{\text{volc}}$ and $\delta^{34}\text{S}_{\text{anthro}}$. The Keeling Plot determination of $\delta^{34}\text{S}_{\text{volc}}$ and $\delta^{34}\text{S}_{\text{anthro}}$ in Figures S4b and S4d is a more regionally representative determination of $\delta^{34}\text{S}_{\text{volc}}$ and $\delta^{34}\text{S}_{\text{anthro}}$ because the Keeling Plot only represents volcanic and anthropogenic emissions close to Summit, Greenland. The purpose of the compilations of $\delta^{34}\text{S}_{\text{volc}}$ and $\delta^{34}\text{S}_{\text{anthro}}$ in Figures S4c and S4e is to provide a secondary, independent estimation of $\delta^{34}\text{S}_{\text{volc}}$ and $\delta^{34}\text{S}_{\text{anthro}}$ to compare to the Keeling Plot determination of these source signatures. For the determination of $\delta^{34}\text{S}_{\text{bio}}$, we cannot use a Keeling Plot because it is a less variable source compared to volcanic and anthropogenic sulfur. Instead, we use the global compilation of DMS-derived compounds shown in Figure S4a. Amrani et al. (27) measured DMS-derived compounds from many regions around the globe and found that the isotopic signature of DMS-derived sulfur does not vary significantly geographically.

We recognize that these global compilations include volcanic and coal and oil emissions that are not likely to influence the ice core. For example, emissions from White Island volcano in New Zealand or from oil combustion in Australia are too distant to affect Summit, Greenland. To consider how a subset of the measurements shown in Figures S4a, S4c, and S4e could affect our compilation-based assessment of the source signatures, we limit our analysis to measurements taken from the back trajectory region (34): $45^\circ - 90^\circ \text{ N}$, $120^\circ \text{ W} - 30^\circ \text{ E}$. The mean of this subset of measurements from the back trajectory region is shown as a dashed line in Figures S4a, S4c, and S4e. The mean signature of the back-trajectory subset of each compilation ($\delta^{34}\text{S}_{\text{anthro}} = +2.0 \text{ ‰}$, $\delta^{34}\text{S}_{\text{volc}} = +2.5 \text{ ‰}$, and $\delta^{34}\text{S}_{\text{bio}} = +20.5 \text{ ‰}$) are similar to the mean of the global compilation ($\delta^{34}\text{S}_{\text{anthro}} = +3.4 \text{ ‰}$, $\delta^{34}\text{S}_{\text{volc}} = +3.8 \text{ ‰}$, and $\delta^{34}\text{S}_{\text{bio}} = +18.8 \text{ ‰}$) considering the limited number of observations in the back-trajectory subset (e.g., $N = 5$ for volcanic gas $\delta^{34}\text{S}$ measurements in the back trajectory region). Furthermore, the overall results of this study are not qualitatively different when using these signatures. For example, the change in total bioS from the preindustrial to the industrial era estimated using the

Keeling Plot signatures is a change of 3.8 to 4.5 $\mu\text{g S kg}^{-1}$ (an increase of 18%). The change in total bioS from the preindustrial to the industrial era estimated using the subset of the compilation (dashed lines in Figures S4a, S4c, and S4e) is 3.6 to 4.0 $\mu\text{g S kg}^{-1}$ (an increase of 13%). The increase of 18% vs. 13% is qualitatively similar because $\delta^{34}\text{S}_{\text{bio}}$ is very distinct from $\delta^{34}\text{S}_{\text{volc}}$ and $\delta^{34}\text{S}_{\text{anthro}}$.

However, these global and back trajectory subset compilations are not used to determine the volcanic, biogenic, and anthropogenic sulfate fractions (Figure 1) and concentrations (Figures 2 and 3). We primarily use the Keeling Plot determination of source signatures to determine the volcanic, biogenic, and anthropogenic fractions of ice core non-sea salt sulfate because the Keeling Plot represents a regional signal weighted by individual source fluxes (i.e., only volcanoes and fossil fuel combustion that influence Greenland) and inherently includes possible fractionation due to transport and oxidation.

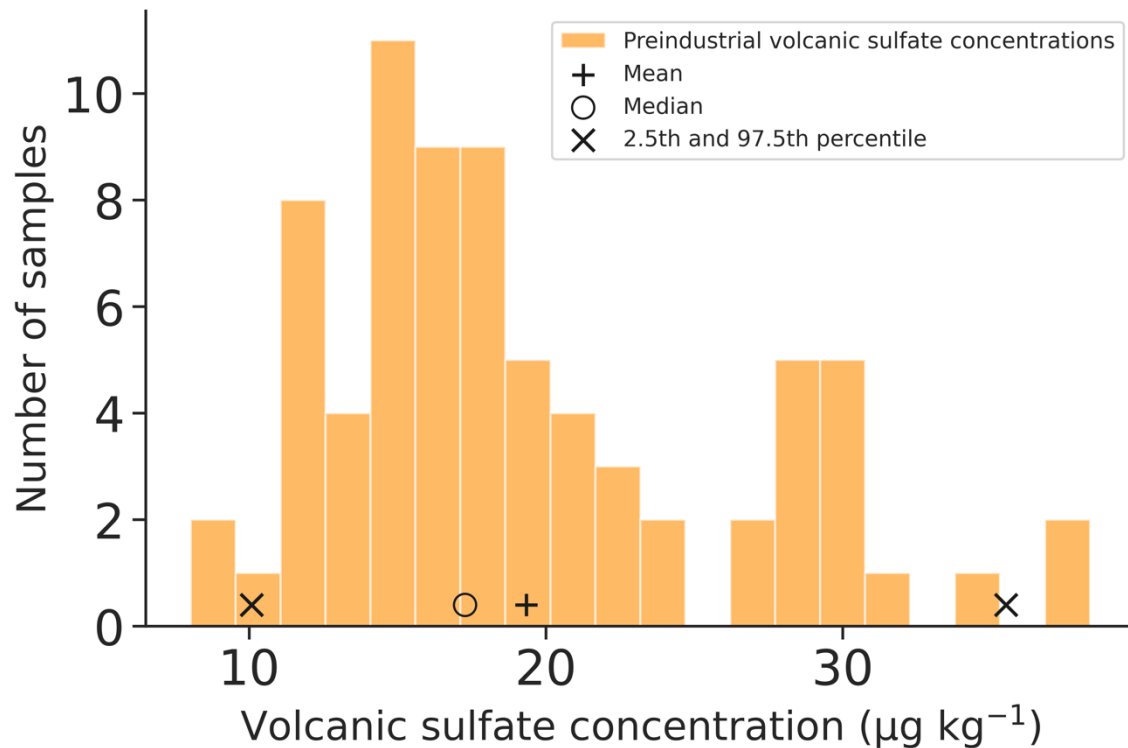


Figure S2. Distribution of preindustrial volcanic sulfate concentrations with markers outlining the preindustrial mean, median, 92.5th, and 97.5th percentile. The assumed volcanic sulfate concentration in the industrial era is equal to the median preindustrial volcanic sulfate concentration (marked with a circle). A range of the mean \pm 2 standard deviations around the mean preindustrial volcanic sulfate concentration (i.e. the 2.5th and 97.5th percentiles) is also assumed to estimate a range in industrial-era biogenic sulfate concentrations. The range in biogenic sulfate concentrations is shown in Figures S3 and S4.

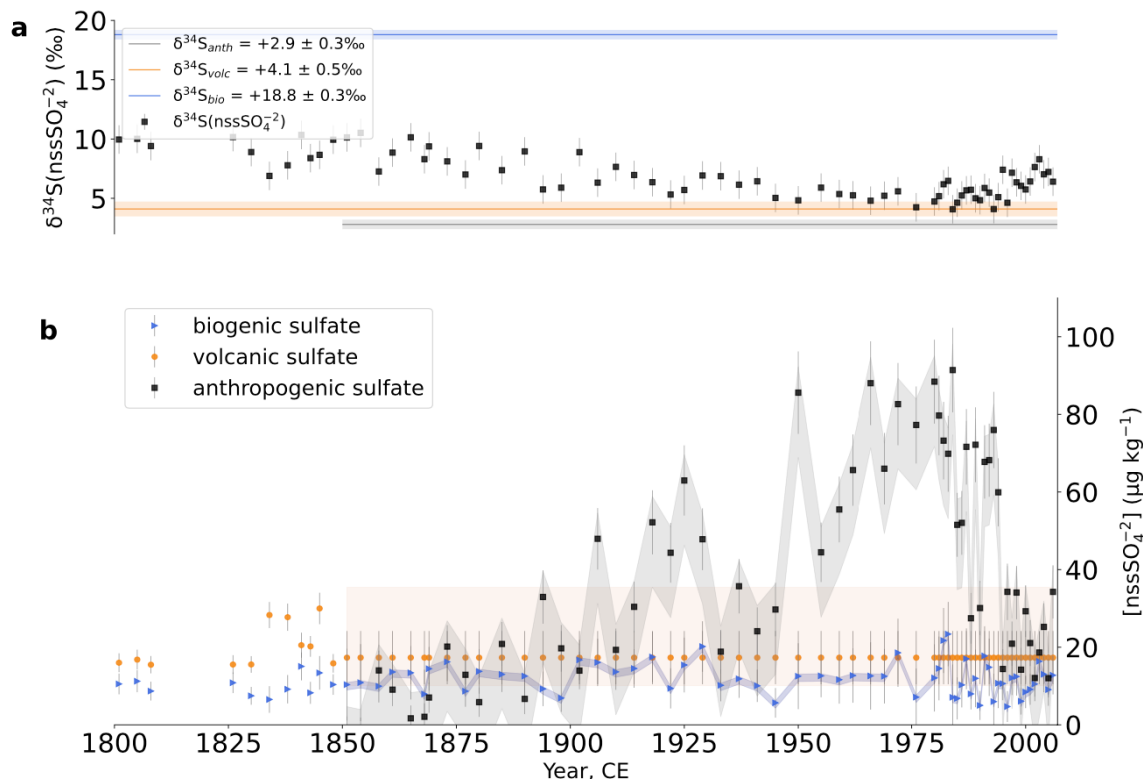
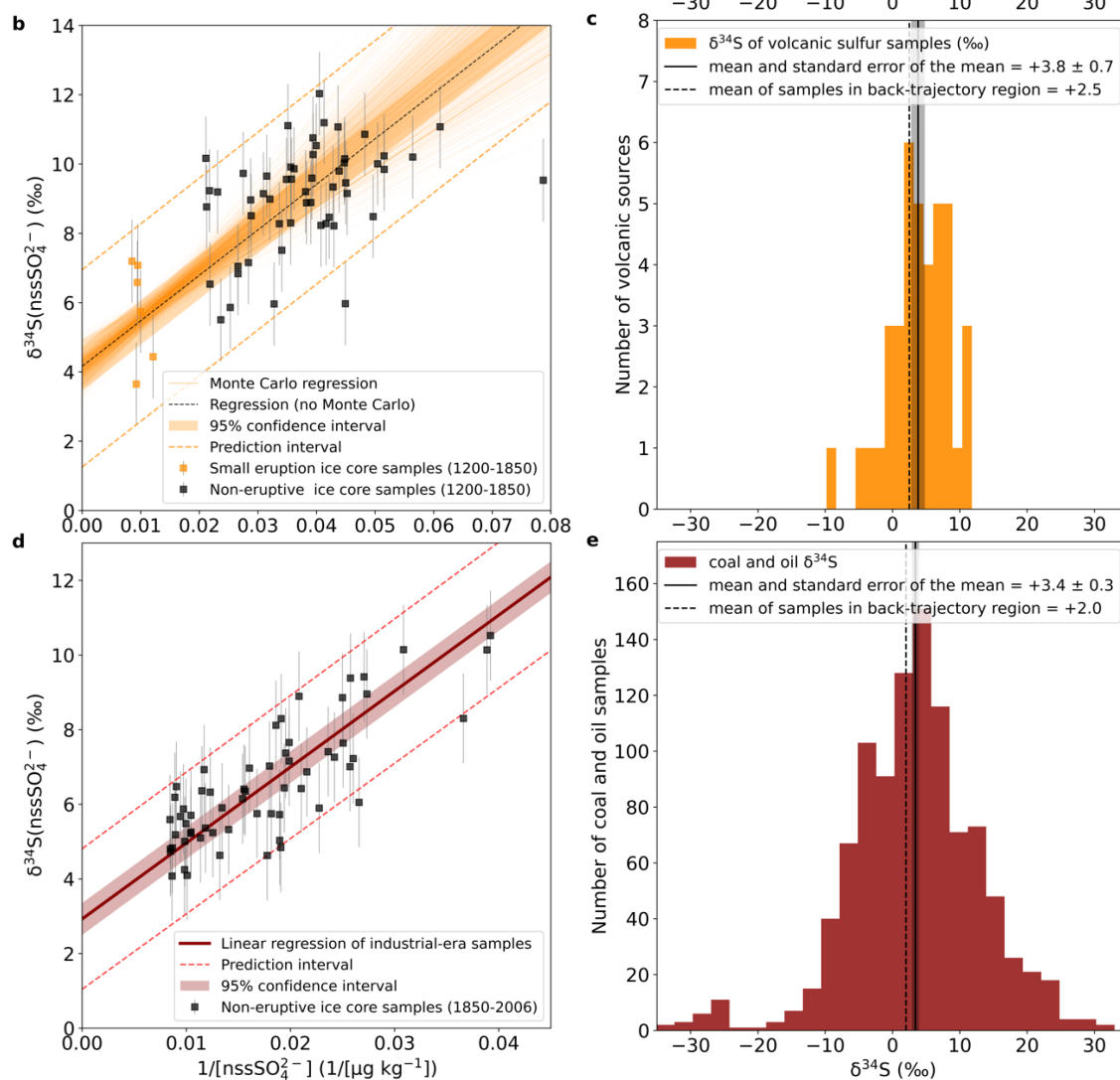


Figure S3. Range in estimated anthropogenic (gray) and biogenic (blue) sulfate concentrations over the industrial era depending on assumed volcanic (orange) sulfate concentrations. a) Sulfur isotopic composition ($\delta^{34}\text{S}$) of non-sea salt sulfate (‰) with colored lines indicating specific isotopic composition of anthropogenic (gray), biogenic (blue) and volcanic (orange) sources. b) anthropogenic (black markers) and biogenic (blue markers) sulfate concentrations estimated assuming that volcanic sulfate concentrations are equal to the median preindustrial volcanic sulfate concentrations (orange markers). The shaded regions show the range in biogenic (blue shaded) and anthropogenic (gray shaded) sulfate concentrations assuming the 2.5th and 97.5th percentile preindustrial volcanic sulfate concentration (orange shaded). The biogenic sulfur isotopic signature ($\delta^{34}\text{S}_{\text{bio}} = +18.8 \pm 0.3 \text{‰}$) is distinct from the volcanic and anthropogenic sulfur isotopic signatures ($\delta^{34}\text{S}_{\text{volc}} = +4.1 \pm 0.5 \text{‰}$ and $\delta^{34}\text{S}_{\text{anthro}} = +2.9 \pm 0.3 \text{‰}$), and thus the wide range in possible volcanic sulfate concentrations during the industrial era contributes only 28% of the total uncertainty in estimated biogenic sulfate concentrations. The trends in anthropogenic sulfate concentrations are discussed in Jongebloed et al. (4).

Figure S4. Determination of $\delta^{34}\text{S}$ signatures from biogenic, volcanic, and anthropogenic sulfur from Jongeblod et al. (2, 4). (a) Determination of $\delta^{34}\text{S}_{\text{bio}} = +18.8 \pm 0.3 \text{‰}$ via compilation of direct measurements of DMS and its precursors and oxidation products with mean back-trajectory region $\delta^{34}\text{S}_{\text{bio}} = +20.5 \text{‰}$; (b) determination of $\delta^{34}\text{S}_{\text{volc}} = +4.1 \pm 0.5 \text{‰}$ through Keeling Plot; (c) determination of $\delta^{34}\text{S}_{\text{volc}} = +3.8 \pm 0.7 \text{‰}$ through compilation of direct measurements of volcanic gases from around the world and $\delta^{34}\text{S}_{\text{volc}} = +2.5 \text{‰}$ from volcanoes in the back-trajectory region; (d) determination of $\delta^{34}\text{S}_{\text{anthro}} = +2.9 \pm 0.3 \text{‰}$ through Keeling Plot; (e) determination of $\delta^{34}\text{S}_{\text{anthro}} = +3.4 \pm 0.3 \text{‰}$ through compilation of direct measurements of coal and oil $\delta^{34}\text{S}$ from around the world and $\delta^{34}\text{S}_{\text{anthro}} = +2.0 \text{‰}$ from coal and oil in the back-trajectory region. Prediction interval and 95% confidence interval for the Keeling Plot regressions in (b) and (c) are shown with dashed lines and a shaded region, respectively, and discussed in Supplementary Text S3. Details on Keeling Plots and direct measurements are in Supplementary Text S3 and in Jongeblod et al. (2, 4).



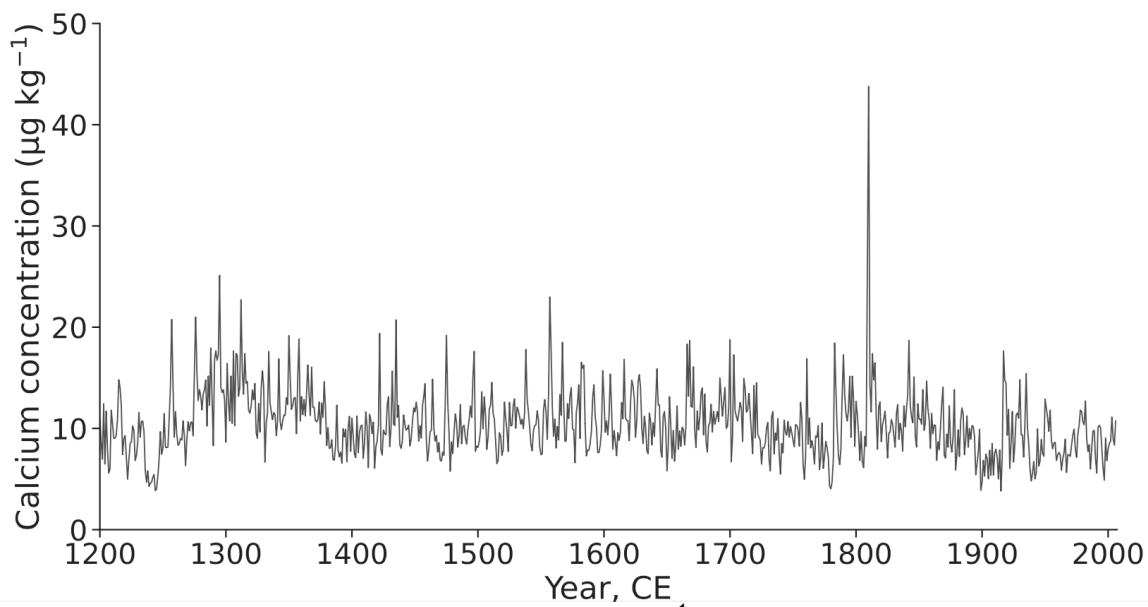


Figure S5. Annual concentrations of calcium ($\mu\text{g kg}^{-1}$) in ice core samples from Summit, Greenland from 1200 to 2006 CE.

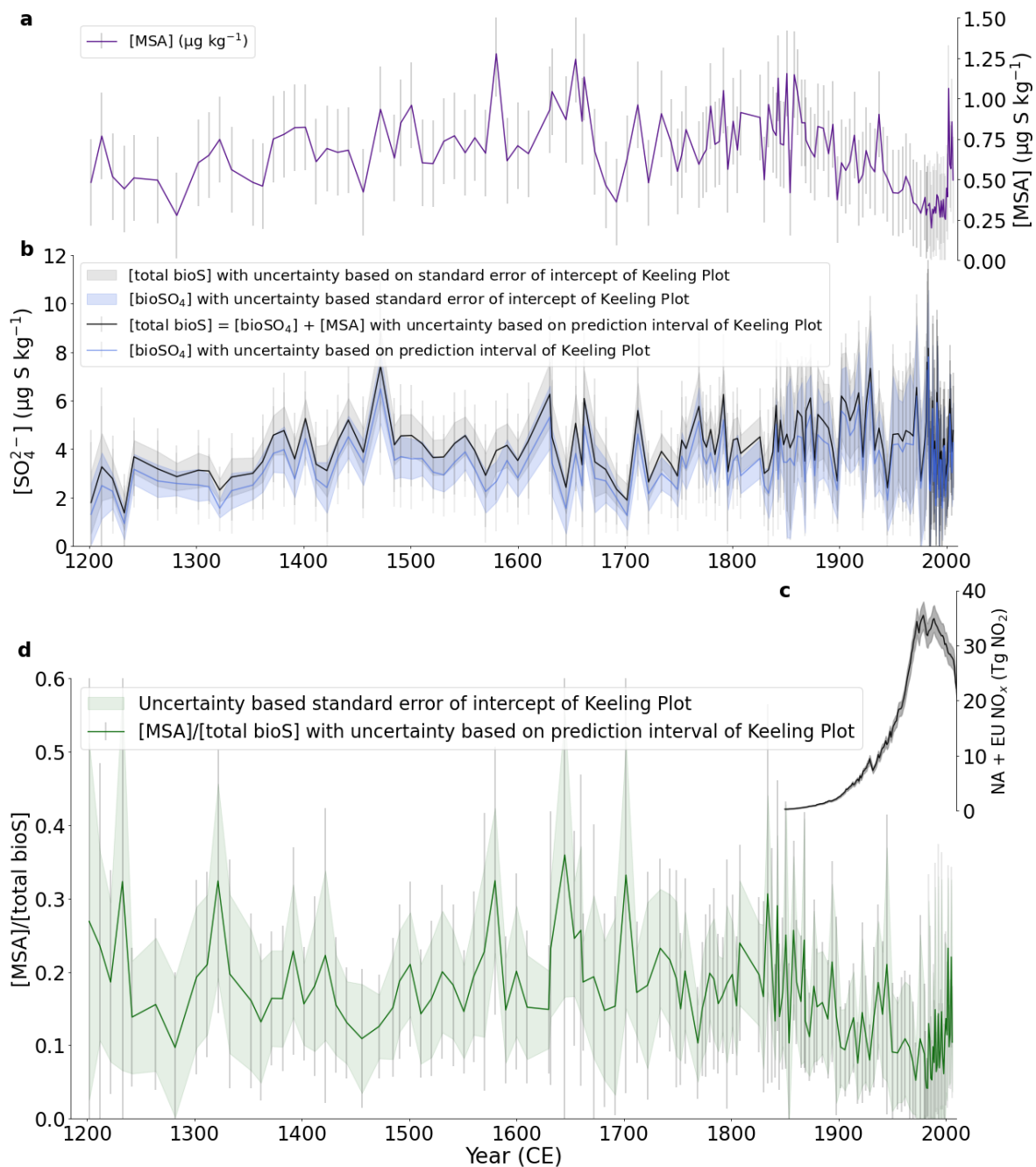


Figure S6. Same as Figure 2 in main text, but with uncertainty estimated based on the prediction intervals in Figure S4b and S4d (error bars in Figure S5b and S5d) and uncertainty estimated based on the standard error of the intercept in Figure S4b and S4d (shaded regions shown in Figure S5b and S5d).

Supplementary Information References

1. E. Ruggieri, A Bayesian approach to detecting change points in climatic records. *International Journal of Climatology* **33**, 520–528 (2013).
2. U. A. Jongebloed, *et al.*, Underestimated Passive Volcanic Sulfur Degassing Implies Overestimated Anthropogenic Aerosol Forcing. *Geophys Res Lett* **50** (2023).
3. J. Cole-Dai, D. M. Budner, D. G. Ferris, High speed, high resolution, and continuous chemical analysis of ice cores using a melter and ion chromatography. *Environ Sci Technol* **40**, 6764–6769 (2006).
4. U. A. Jongebloed, *et al.*, Sulfur isotopes quantify the impact of anthropogenic activities on industrial-era Arctic sulfate in a Greenland ice core. *Environmental Research Letters* (2023) <https://doi.org/https://doi.org/10.1088/1748-9326/acdc3d>.
5. J. Cole-Dai, *et al.*, Two likely stratospheric volcanic eruptions in the 1450s C.E. found in a bipolar, subannually dated 800 year ice core record. *Journal of Geophysical Research Atmospheres* **118**, 7459–7466 (2013).
6. E. le Gendre, E. Martin, B. Villemant, P. Cartigny, N. Assayag, A simple and reliable anion-exchange resin method for sulfate extraction and purification suitable for multiple O- and S-isotope measurements. *Rapid Communications in Mass Spectrometry* **31**, 137–144 (2017).
7. B. Fry, S. R. Silva, C. Kendall, R. K. Anderson, Oxygen isotope corrections for online $\delta^{34}\text{S}$ analysis. *Rapid Communications in Mass Spectrometry* **16**, 854–858 (2002).
8. J. P. D. Abbatt, *et al.*, Overview paper: New insights into aerosol and climate in the Arctic. *Atmos Chem Phys* **19**, 2527–2560 (2019).
9. V. Wasiuta, A.-L. Norman, S. Marshall, Spatial patterns and seasonal variation of snowpack sulphate isotopes of the Prince of Wales Icefield, Ellesmere Island, Canada. *Ann Glaciol* **43**, 390–396 (2006).
10. R. Ghahremaninezhad, A. L. Norman, J. P. D. Abbatt, M. Levasseur, J. L. Thomas, Biogenic, anthropogenic and sea salt sulfate size-segregated aerosols in the Arctic summer. *Atmos Chem Phys* **16**, 5191–5202 (2016).
11. A. L. Norman, *et al.*, Sources of aerosol sulphate at Alert: apportionment using stable isotopes. *J Geophys Res* **104**, 11,619–11,631 (1999).
12. N. Patris, *et al.*, First sulfur isotope measurements in central Greenland ice cores along the preindustrial and industrial periods. *Journal of Geophysical Research: Atmospheres* **107** (2002).
13. M. Sigl, *et al.*, A new bipolar ice core record of volcanism from WAIS Divide and NEEM and implications for climate forcing of the last 2000 years. *Journal of Geophysical Research Atmospheres* **118**, 1151–1169 (2013).
14. R. Uemura, *et al.*, Soluble salts in deserts as a source of sulfate aerosols in an Antarctic ice core during the last glacial period. *Earth Planet Sci Lett* **578** (2022).
15. A. J. M. Bory, P. E. Biscaye, A. M. Piotrowski, J. P. Steffensen, Regional variability of ice core dust composition and provenance in Greenland. *Geochemistry, Geophysics, Geosystems* **4** (2003).
16. C. Klein, C. Hurlbut, “Systematic Mineralogy Part IV: Silicates” in *Manual of Mineralogy*, 20th Ed., (John Wiley & Sons, 1985), pp. 366–467.

17. Y. Iizuka, *et al.*, A 60 Year Record of Atmospheric Aerosol Depositions Preserved in a High-Accumulation Dome Ice Core, Southeast Greenland. *Journal of Geophysical Research: Atmospheres* **123**, 574–589 (2018).
18. D. E. Pataki, *et al.*, The application and interpretation of Keeling plots in terrestrial carbon cycle research. *Global Biogeochem Cycles* **17**, 1022 (2003).
19. C. D. Keeling, The concentration and isotopic abundances of atmospheric carbon dioxide in rural areas. *Geochim Cosmochim Acta* **13**, 322 (1958).
20. C. D. Keeling, *et al.*, “A three-dimensional model of atmospheric CO₂ transport based on observed winds: 1. Analysis of observational data” in *Aspects of Climate Variability in the Pacific and the Western Americas*, D. H. Peterson, Ed. (AGU, 1989), pp. 165–236.
21. J. M. de Moor, *et al.*, Sulfur isotope fractionation during the May 2003 eruption of Anatahan volcano, Mariana Islands: Implications for sulfur sources and plume processes. *Geochim Cosmochim Acta* **74**, 5382–5397 (2010).
22. N. Patris, R. J. Delmas, J. Jouzel, Isotopic signatures of sulfur in shallow Antarctic ice cores. *Journal of Geophysical Research Atmospheres* **105**, 7071–7078 (2000).
23. S. A. Kunasek, *et al.*, Sulfate sources and oxidation chemistry over the past 230 years from sulfur and oxygen isotopes of sulfate in a West Antarctic ice core. *Journal of Geophysical Research Atmospheres* **115** (2010).
24. H. Nielsen, *et al.*, *Lithospheric Sources of Sulphur*, H. R. Krouse, V. A. Grinenko, Eds. (John Wiley, 1991).
25. C. Kern, A. Aiuppa, J. M. de Moor, A golden era for volcanic gas geochemistry? *Bull Volcanol* **84**, 43 (2022).
26. V. Wasiuta, M. J. Lafrenière, A. L. Norman, M. G. Hastings, Summer deposition of sulfate and reactive nitrogen to two alpine valleys in the Canadian Rocky Mountains. *Atmos Environ* **101**, 270–285 (2015).
27. A. Amrani, W. Said-Ahmad, Y. Shaked, R. P. Kiene, Sulfur isotope homogeneity of oceanic DMSP and DMS. *Proc Natl Acad Sci U S A* **110**, 18413–18418 (2013).
28. M. E. Böttcher, H. J. Brumsack, C. D. Dürselen, The isotopic composition of modern seawater sulfate: I. Coastal waters with special regard to the North Sea. *Journal of Marine Systems* **67**, 73–82 (2007).
29. C. E. Rees, W. J. Jenkins, J. Monster, The sulphur isotopic composition of ocean water sulphate*. *Geochim Cosmochim Acta* **42**, 377–381 (1978).
30. G. Carnat, *et al.*, Variability in sulfur isotope composition suggests unique dimethylsulfoniopropionate cycling and microalgae metabolism in Antarctic sea ice. *Commun Biol* **1** (2018).
31. S. Li, L. A. Barrie, Biogenic Sulfur Aerosol in the Arctic Troposphere: 1. Contributions to Total Sulfate. *J Geophys Res* **98**, 613–633 (1993).
32. J. O Nriagu, R. D. Coker, Isotopic composition of sulfur in precipitation within the Great Lakes Basin. *Tellus* **30**, 365–375 (1978).
33. L. Wasserman, “Prediction” in *All of Statistics*, (2004), pp. 214–215.
34. S. Zhai, *et al.*, Anthropogenic Impacts on Tropospheric Reactive Chlorine Since the Preindustrial. *Geophys Res Lett* **48** (2021).